optica

Further improvements to the ptychographical iterative engine: supplementary material

ANDREW MAIDEN*, DANIEL JOHNSON, AND PENG LI

Department of Electronic and Electrical Engineering, University of Sheffield, Sheffield, S1 3JD, UK
**Corresponding author: a.maiden@sheffield.ac.uk*

Published 30 June 2017

This document provides supplementary information to "Further improvements to the ptychographical iterative engine," https://doi.org/10.1364/optica.4.000736. We describe the ways in which a ptychographic reconstruction can be affected by inherent ambiguities, then show how to compensate for them in order to realize an accurate real-world error metric in simulated experiments. We also demonstrate two straightforward additions to the reconstruction algorithm that improve robustness by preventing some of these ambiguities from occurring.

https://doi.org/10.1364/optica.4.000736.s001

1. An error metric for simulations

There are several possible ambiguities between the underlying 'ground truth' of a ptychographic experiment or simulation and the reconstructed object and probe: a constant amplitude scaling, a constant phase offset, a global real-space translation and a linear phase ramp. (We have ignored the periodic artefacts that can arise when ptychographic data is collected from a regular square grid of positions – the 'raster grid pathology' – since the careful experimenter chooses a scan pattern to avoid this possibility [1].) Equation S1 summarizes the ambiguities:

$$\psi_{j\mathbf{r}} = P_{j\mathbf{r}} o_{j\mathbf{r}} = \left(a e^{jc} e^{j\mathbf{b}\cdot\mathbf{r}} \hat{P}_{\mathbf{r}+\mathbf{d}}\right)\left(a^{-1} e^{-jc} e^{-j\mathbf{b}\cdot\mathbf{r}} \hat{O}_{\mathbf{x}_j+\mathbf{d}}\right) \quad \textbf{(S1)}$$

Here the hatted variables, $\hat{P}_{\mathbf{r}}$ and $\hat{O}_{\mathbf{x}}$, represent the true probe and object respectively, a and c are scalar constants, and $\mathbf{b}$ and $\mathbf{d}$ are constant vectors.

For the most part, these ambiguities are inconsequential. However, the amplitude scaling can cause problems when the reconstruction process enters a cycle in which the parameter a slowly grows from iteration to iteration. This is a feature we have observed to severely affect the PIE algorithm for low values of its tuning parameter, α, and also occurs where diffraction patterns in an experiment contain a high level of readout noise (a pedestal). Although often overlooked in the literature, the phase ramp ambiguity can also be problematic, especially for large-area ptychographic scans where even a very shallow ramp can distort the reconstruction [2]. For 3D ptychography the ambiguities can be especially unhelpful, since in this case the projections reconstructed from many ptychographic scans must be recombined using tomographic methods and each projection is likely to be disturbed by the ambiguities in different ways. To avoid this, each projection must be aligned to eliminate any real-space translation (the parameter $\mathbf{d}$ in Eq. S1), whilst a region of free-space adjacent to the specimen should be scanned during the experiment to ensure equal values in each projection for the other parameters, a, $\mathbf{b}$ and c [3].

To measure the performance of a reconstruction algorithm via simulation, all of the ambiguities in Eq. S1 must be factored in to any real space error metric. To accomplish this, we adopt a step-by-step approach to remove the ambiguities from the reconstructed object, $O_{j\mathbf{x}}$, creating the unambiguous object estimate, $O_{j\mathbf{x}}^{(\mathrm{unamb})}$.

The process is:

1) Estimate the global translation ($\mathbf{d}$ in Eq. S1) of the object and probe by cross-correlation, to sub-pixel precision, of the ground truth and reconstructed probe amplitudes. We use the indispensable method and code from Guizar-Sicairos for the cross-correlation [4].

2) Initialise $O_{j\mathbf{x}}^{(\mathrm{unamb})}$ to $O_{j\mathbf{x}}$, and shift it by the negative of the estimated value of $\mathbf{d}$ from step 1.

3) Extract a central region, the subset of pixels $\mathbf{x}_c$, from $\hat{O}_{\mathbf{x}}$ and $O_{j\mathbf{x}}^{(\mathrm{unamb})}$: this 'good' reconstruction region will be used to derive the error value.

4) Estimate any phase ramp, i.e. parameter **b**, as follows:

   a. Calculate:

$$\mathcal{F}\left[\exp\left(j\angle\left(O_{j\mathbf{x}_c}^{(\text{unamb})}\hat{O}_{\mathbf{x}_c}^{*}\right)\right)\right] \quad \textbf{(S2)}$$

   Where $\mathcal{F}$ is the Fourier transform,

   b. Locate, with sub-pixel precision, the maximum of Eq. S2, to give an approximation to **b** in Eq. S1. (We implement this by cross-correlation with a matrix of ones, using the method as in Step 1.)

5) Apply a compensating phase ramp to $O_{j\mathbf{x}_c}^{(\text{unamb})}$.

6) Estimate the global scaling factor:

$$ae^{j\gamma} \approx \gamma = \frac{\sum_{\mathbf{x}_c} O_{j\mathbf{x}_c}^{(\text{unamb})}\hat{O}_{\mathbf{x}_c}^{*}}{\sum_{\mathbf{x}_c}\left|\hat{O}_{\mathbf{x}_c}\right|^2} \quad \textbf{(S3)}$$

7) Divide $O_{j\mathbf{x}_c}^{(\text{unamb})}$ by γ.

Having removed all of the ambiguities in this way, the normalized error between the estimate and true object is:

$$E_{\text{sim}} = \frac{\sum_{\mathbf{x}_c}\left|\hat{O}_{\mathbf{x}_c} - O_{j\mathbf{x}_c}^{(\text{unamb})}\right|^2}{\sum_{\mathbf{x}_c}\left|\hat{O}_{\mathbf{x}_c}\right|^2} \quad \textbf{(S4)}$$

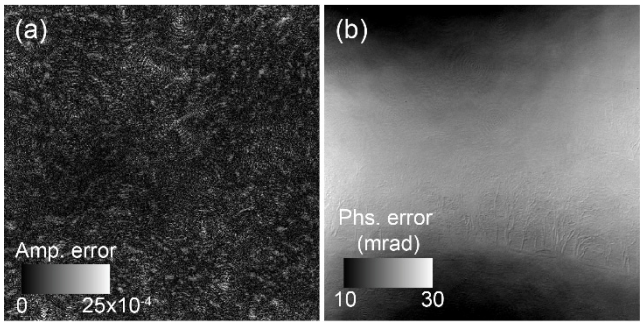

Fig. S1. An ePIE reconstruction was carried out using data from a simulated soft X-ray experiment. The Figure shows the difference between the (a) amplitude and (b) phase of the true object and the reconstructed object with all ambiguities removed. The phase difference highlights the problem ptychography faces in reconstructing very low frequency phase components.

It is interesting to image the difference between the amplitude and phase of the true object in a simulation and that of $O_{j\mathbf{x}_c}^{(\text{unamb})}$. Fig. S1 shows these differences for an ePIE reconstruction of the soft X-ray simulation described in the primary manuscript (Fig. 7), where the initial probe for the reconstruction was this time given the correct defocus of 750μm. The amplitude difference in Fig. S1a is essentially random, with some slight ringing artefacts corresponding to structures in the probe. Although the phase of the reconstructed object is visually close to the true object, the phase difference between them, shown in Fig. S1b, is dominated by a low frequency modulation, which results from the difficulty ptychography faces in linking highly disconnected regions of the reconstruction. An area for further investigation is to determine whether the diffraction pattern order can be tailored to help synchronize the phases of widely separated parts of the object to avoid these low frequency errors [5].

2. Enhancements to the probe update

With two additions to the probe update described in the primary manuscript, it is possible to eliminate two of the ambiguities in Eq. S1. We have found both additions beneficial for real world data, especially where the recorded diffraction patterns are noisy and/or when the probe is highly structured.

A. Power correction

Our first addition corrects the probe's power to a predefined value as the reconstruction iterates, eliminating the scale-factor ambiguity represented by *a* in Eq. S1. The predefined probe power can be determined by measuring a diffraction pattern from the experimental setup prior to inserting the specimen, and summing its intensity over every pixel, or more simply by summing the pixel intensities of the brightest diffraction pattern from the ptychographic data set, which gives a good-enough estimate of the power.

We have found it best to implement the power correction *after* calculation of the revised exit-wave (See Fig. 1 of the primary manuscript), i.e. immediately before the probe and object updates are carried out. For a far-field diffraction pattern, the power correction step is:

$$P_{j\mathbf{r}} \leftarrow P_{j\mathbf{r}}\sqrt{\frac{\sum_{\mathbf{u}}\left|I_{\mathbf{u}}^{(\text{ref})}\right|^2}{NM\sum_{\mathbf{r}}\left|P_{j\mathbf{r}}\right|^2}} \quad \textbf{(S5)}$$

Where $I_{\mathbf{u}}^{(\text{ref})}$ is the chosen reference diffraction pattern. Note that the numerator in Eq. S5 can be pre-computed, and for near-field propagators where two Fourier transform operations are required, e.g. the Angular Spectrum, the factor *NM* should be removed. We have found that correcting the probe power via Eq. S5 is more effective than the alternate strategy of limiting the object amplitude to a narrow range; Fig. S2 gives a real-world example of its utility.

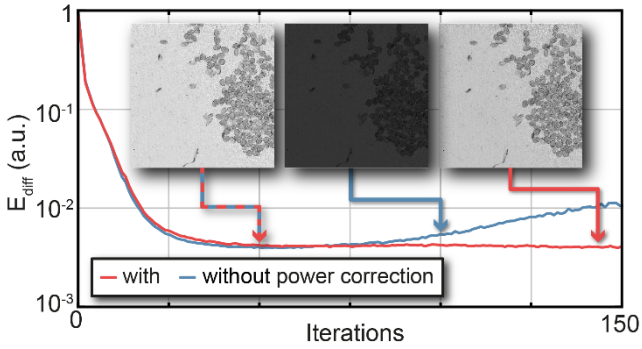

Fig. S2. Especially where there is significant readout noise in an a ptychographic experiment, reconstruction algorithms can enter a cycle where the object estimate slowly reduces in intensity, eventually causing the algorithm to destabilize. To remedy this problem, the ambiguity that causes it can be eliminated by correcting the probe power to a reference value.

B. Probe centering

Our second addition takes the regularization idea from the primary manuscript further, by adding a third term into the error metric of Eq. 13 that penalizes high probe intensities according to a

spatially varying weight. Its purpose is to remove the global translation ambiguity, represented by the vector **d** in Eq. S1, by 'encouraging' the probe to remain centered in its reconstruction window. The regularized cost function with the additional term is:

$$E_P^{(\mathrm{reg})} = \sum_{\mathbf{r}} \left| P'_{j\mathbf{r}} o_{j\mathbf{r}} - \psi'_{j\mathbf{r}} \right|^2 + \sum_{\mathbf{r}} v_{j\mathbf{r}} \left| P'_{j\mathbf{r}} - P_{j\mathbf{r}} \right|^2 + \sum_{\mathbf{r}} b_{\mathbf{r}} \left| P'_{j\mathbf{r}} \right|^2 \quad \textbf{(S6)}$$

Here, $v_{j\mathbf{r}}$ is the regularization weighting – the probe-update-equivalent of $w_{j\mathbf{r}}$ from the primary manuscript – and $b_{\mathbf{r}}$ is chosen with zero at its center, rising to a larger value toward the edges of the probe window: this imposes an increased penalty whenever the probe has high intensities towards its periphery. The derivative of Eq. S6 is:

$$\frac{1}{2}\nabla E_P^{(\mathrm{reg})} = o_{j\mathbf{r}}^* \left(P'_{j\mathbf{r}} o_{j\mathbf{r}} - \psi'_{j\mathbf{r}} \right) + v_{j\mathbf{r}} \left(P'_{j\mathbf{r}} - P_{j\mathbf{r}} \right) + b_{\mathbf{r}} P'_{j\mathbf{r}} \quad \textbf{(S7)}$$

Setting this derivative to zero and solving for the new probe gives:

$$P'_{j\mathbf{r}} = P_{j\mathbf{r}} + \frac{o_{j\mathbf{r}}^* \left(\psi'_{j\mathbf{r}} - \psi_{j\mathbf{r}} \right) - b_{\mathbf{r}} P_{j\mathbf{r}}}{\left| o_{j\mathbf{r}} \right|^2 + v_{j\mathbf{r}} + b_{\mathbf{r}}} \quad \textbf{(S8)}$$

The function $v_{j\mathbf{r}}$ is defined by the reconstruction algorithm and the probe tuning parameter β (see Table 1 of the primary manuscript). $b_{\mathbf{r}}$ can simply be a disc of zeros in a matrix of ones, or we have used a smoothed disc effectively, as in Fig S3 which shows an example of the probe centering in operation. We have found keeping the probe central in this way more reliable than shifting the probe center of mass at each update [6].

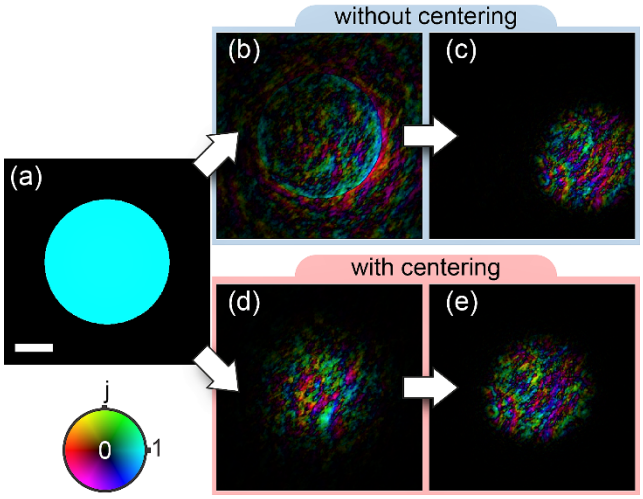

Fig. S3. In this experiment, a diffuser was used to give a highly structured probe. (a) The initial probe estimate of an empty aperture is far distant from the true probe. (b) After two iterations of ePIE without probe recentering, the probe estimate breaks up, before (c) reforming off-centre after 50 iterations; errors in the probe where it nears the edge of the reconstruction window distorted the final object reconstruction. (d) With probe recentering active, the probe is contained near the center after two iterations. (e) The recentering is turned off after 10 iterations, but by this time the probe is reasonably well defined and after 50 iterations remains well centered. Scale bar 200μm, complex-valued probes represented using the colorwheel shown.

References

1. X. Huang, H. Yan, R. Harder, Y. Hwu, I. K. Robinson, and Y. S. Chu, "Optimization of overlap uniformness for ptychography," Optics Express **22**, 12634-12644 (2014).
2. S. McDermott, P. Li, G. Williams, and A. Maiden, "Characterizing a spatial light modulator using ptychography," Optics Letters **42**, 371-374 (2017).
3. M. Guizar-Sicairos, A. Diaz, M. Holler, M. S. Lucas, A. Menzel, R. A. Wepf, and O. Bunk, "Phase tomography from x-ray coherent diffractive imaging projections," Optics Express **19**, 21345-21357 (2011).
4. M. Guizar-Sicairos, S. T. Thurman, and J. R. Fienup, "Efficient subpixel image registration algorithms," Optics letters **33**, 156-158 (2008).
5. S. Marchesini, A. Schirotzek, C. Yang, H.-t. Wu, and F. Maia, "Augmented projections for ptychographic imaging," Inverse Problems 29, 115009 (2013)
6. S. Marchesini, H. Krishnan, B. J. Daurer, D. A. Shapiro, T. Perciano, J. A. Sethian, and F. R. Maia, "SHARP: a distributed GPU-based ptychographic solver," Journal of Applied Crystallography **49**(2016).